

Entangled X-ray Photon Pair Generation by Free Electron Lasers

Linfeng Zhang^{1†}, Zunqi Li^{1†}, Dongyu Liu^{1,6}, Ming Zhang¹, Chengyin Wu^{1,4,5}, Haitan Xu^{2,3*} and Zheng Li^{1,4,5*}

¹State Key Laboratory for Mesoscopic Physics and Collaborative Innovation Center of Quantum Matter, School of Physics, Peking University, Beijing, 100871, China.

²School of Materials Science and Intelligent Engineering, Nanjing University, Suzhou, 215163, Jiangsu, China.

³Shenzhen Institute for Quantum Science and Engineering, Southern University of Science and Technology, Shenzhen, 518055, Guangdong, China.

⁴Peking University Yangtze Delta Institute of Optoelectronics, Nantong, China.

⁵Collaborative Innovation Center of Extreme Optics, Shanxi University, , Taiyuan, 030006, Shanxi, China.

⁶Physics Department, Stanford University, CA, 94305, USA.

*Corresponding author(s). E-mail(s): haitanxu@nju.edu.cn; zheng.li@pku.edu.cn;

[†]These authors contributed equally to this work.

Einstein, Podolsky and Rosen's prediction [1] on incompleteness of quantum mechanics was overturned by experimental tests on Bell's inequality [2] that confirmed the existence of quantum entanglement. In X-ray optics, entangled photon pairs can be generated by X-ray parametric down conversion (XPDC), which has certain wavelength window [3]. Meanwhile, free electron laser (FEL) has successfully lased at X-ray frequencies recently [4–10]. However, FEL is usually seen as a classical light source, and its quantum effects are considered minor corrections to the classical theory. Here we

investigate entangled X-ray photon pair emissions in FEL. We establish a theory for coherently amplified entangled photon pair emission from microbunched electron pulses in the undulator. We also propose an experimental scheme for the observation of the entangled photon pairs via energy and spatial correlation measurements. Such an entangled X-ray photon pair source is of great importance in quantum optics and other X-ray applications.

Being an ultrabright and ultrashort X-ray laser source, FEL has shed light on various research areas including single particle imaging [11–13], ultrafast X-ray spectroscopy [14–16] and high energy density physics [17–19]. The FEL emission was mostly seen as a classical phenomenon with minor quantum corrections [20]. However, a critical quantum effect, i.e., the quantum entanglement, has never been investigated for the X-ray emission from the FEL.

In this work, we study the entangled X-ray photon pair emission from FEL, which can be enhanced by electron microbunching in the undulator. We start by presenting the quantum electrodynamics (QED) treatment of single-electron photon pair emission process in the undulator and calculate the cross section and the entanglement degree. Then we apply the Feynman rules to microbunched electrons, which takes into account the many-body effect, to analyze the coherent amplification and establish the condition for coherence. We also propose an experimental scheme to observe the entangled photon pairs.

Entangled photons from FEL

We present in Fig. 1 the quantum mechanism of entangled X-ray photon pair emission. Fig. 1a shows a typical SASE FEL process in the lab frame. A relativistic electron pulse travels through an undulator, interacts with the electromagnetic (EM) field of the undulator, resulting in electron microbunching and amplified emission.

To facilitate the study of entangled photon emission from the FEL, we use the electron frame (EF), where the incident electron pulse has a zero initial average velocity. We adopt the frame transformation formalism from the Weizsäcker-Williams method [22], and use the natural units $\hbar = c = \epsilon_0 = 1$. For a helical undulator, $A_{\text{Lab}}^\mu = a(0, \cos(k_u x_{\text{Lab}}^3), \sin(k_u x_{\text{Lab}}^3), 0)$, where $a = B_0/k_u$, B_0 is the amplitude of the undulator field, and $k_u = 2\pi/\lambda_u$ is the spatial frequency of the undulator with a period of λ_u in the lab frame [23]. The undulator field is transformed to a quasi-EM wave in the EF by the Lorentz boost as

$$\begin{aligned} A_{\text{EF}}^\mu &= a(0, \cos[k_u(\gamma\beta x_{\text{EF}}^0 + \gamma x_{\text{EF}}^3)], \\ &\quad \sin[k_u(\gamma\beta x_{\text{EF}}^0 + \gamma x_{\text{EF}}^3)], 0) \\ &= a(0, \cos(k \cdot x_{\text{EF}}), \sin(k \cdot x_{\text{EF}}), 0) , \end{aligned} \tag{1}$$

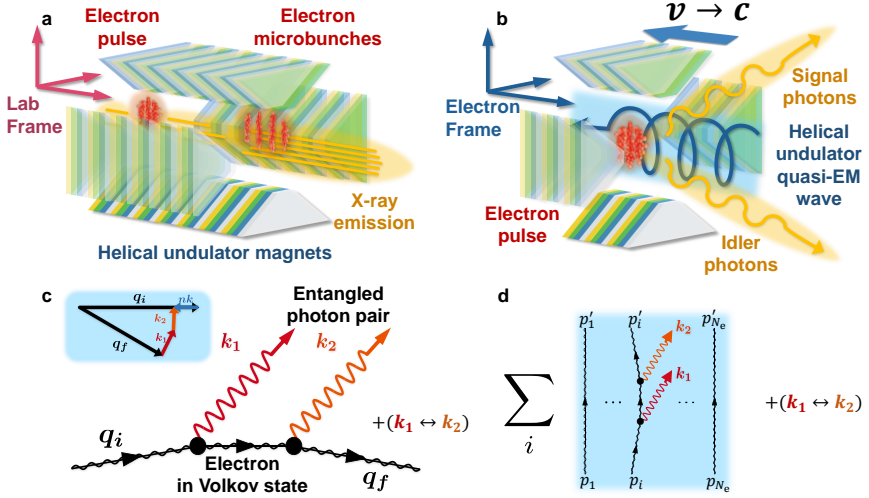


Fig. 1 Mechanism of coherent entangled X-ray photon pair emission in SASE FEL. **a**, Schematic in the lab frame, where a relativistic electron pulse (red) passes through an undulator, causing photon emission (yellow) while being microbunched. The fundamental frequency of the emission can reach X-ray region, with single-photon energy of hundreds of eVs. The schematic of the helical undulator is drawn according to the configuration of the Delta undulator at LCLS [21]. **b**, Schematic in the electron frame, where the electron pulse is initially at rest. The strong quasi-EM wave (blue) of the relativistic undulator is scattered from the electrons. The resulting emission contains multiple components, including single-photon emission, double-photon emission, etc. **c**, The Feynman diagrams corresponding to double-photon emission in the electron frame. The black lines refer to the Volkov states of electron. Inset: a typical constraint of four-momenta of the particles. n is the net number of Floquet photons absorbed. **d**, Coherent summation of Feynman diagrams with $n = 1$, including permutations of k_1 and k_2 .

where β and γ are the average velocity and Lorentz factor of the electron pulse. $k = \gamma k_u(\beta, 0, 0, -1)$ is the wave vector of the undulator quasi-EM wave in the EF, which is close to the photon mass shell for $\beta \rightarrow 1$. The helical undulator is practically available, such as the Delta undulator at LCLS [21].

The SASE emission can be approximated as the scattering of the quasi-EM wave from the electron pulse in the EF. The emission takes part in the microbunching of the electron pulse, and is significantly enhanced at the fundamental frequency and its harmonics. In the lab frame, the fundamental frequency $\omega_{fd} = 2\gamma^2(2\pi/\lambda_u)/(1 + K^2)$ for the helical undulator, where $K = eB_0/mk_u = ea/m$ is the undulator parameter [4, 20, 24].

For strong undulator quasi-EM wave, nonlinear scattering can be observed in the emission. We focus on the double-scattering processes, as shown in Fig. 1b. In this work we use the FEL parameters of Linac Coherent Light Source (LCLS) [4], as shown in Table 1.

For a representative electron initially at rest in the EF, it satisfies the Dirac equation $(\not{p} - e\not{A} - m)\Psi = 0$, where $\not{f} = \gamma^\mu f_\mu$, γ^μ are the Dirac matrices, A is the EM four-potential, e is the electron charge, and m is the rest electron mass.

Electron energy	5 GeV	Undulator period number	1392
Charge per pulse	180 pC	Pierce parameter	2×10^{-3}
Peak current	3.4 kA	Fundamental wavelength	2.30 nm
Repetition rate	120 Hz	Saturation peak power	10 GW
Undulator peak field	1.32 T	Emission pulse FWHM	230 fs
Undulator period length	30 mm		

Table 1 FEL parameters used in this work, based on LCLS [4].

In the undulator quasi-EM wave, the electron is in a Volkov state $\Psi_p^V(x) = (1 - \frac{eA\mathbf{k}}{2k \cdot p})u_p \times \exp\{-i[p \cdot x + \int_0^\phi (\frac{ep \cdot A(\phi')}{k \cdot p} - \frac{e^2 A^2(\phi')}{2k \cdot p})d\phi']\}$, where $\phi = k \cdot x = k^\mu x_\mu = k^0 x^0 - \mathbf{k} \cdot \mathbf{x}$, u_p is the free electron spinor, and $A \simeq A_{\text{EF}}$ [see Section I of Supplementary Information (SI) for details]. For an electron of initial four-momentum p , the corresponding Volkov state has a time-varying four-momentum whose average is the quasi-momentum $q^\mu = p^\mu + \frac{e^2 a^2}{2k \cdot p} k^\mu$, satisfying $|q|^2 = m^2 + e^2 a^2 = m_*^2$.

In the Floquet picture, the Volkov state corresponds to the superposition state of the electron dressed by \tilde{n} Floquet photons, i.e., $\Psi_p^V(x) = \sum_{\tilde{n}=-\infty}^{+\infty} F_{\tilde{n}} \exp\{-i(q \cdot x + \tilde{n}k \cdot x)\}u(p)$ (the expression of $F_{\tilde{n}}$ can be found in SI). The electron in the Volkov state can spontaneously decay into another Volkov state with a different quasi-momentum and thus radiate photons, the amplitude of which can be evaluated by the Feynman diagrams (see details in Section II of SI). Especially, the entangled photon pair emission is equivalent to non-perturbative double Compton scattering of the quasi-EM wave from the electron in the EF [25, 26], which satisfies the four-momentum conservation $q_f + k_1 + k_2 - q_i - nk = 0$ (see Fig. 1c). k_1 and k_2 are the momentum of entangled photons, and n corresponds to the number of Floquet photons absorbed. As the energies of photons (k^0, k_1^0, k_2^0) are much less than the electron mass (m) and the quasi-momenta (q_i, q_f) in the EF when n is reasonably small, the four-momentum conservation leads to $k_1^0 + k_2^0 \simeq nk^0$. We focus on the representative case of $n = 1$, which corresponds to photon pairs with total frequency of ω_{fd} in the lab frame, and can be distinguished from other cases with different n by detecting the emitted photon pair energies (see details in Section III of SI).

With the above treatment, we obtain the scattering matrix element S_{fi} for the process from an initial Volkov state i to any final Volkov state f emitting a pair of photons in plane wave states with arbitrary polarization or helicity. From this, we can further obtain the total scattering rate \dot{W} which reflects the probability of observing the double-photon emission in unit time, and the density matrix ρ_f that describes the joint polarization or helicity state of the emitted photon pair (see details in Methods and Section III of SI). The density matrix of the emitted photon pair ρ_f can be expressed as $\rho_f = \frac{1}{2} \sum_{r_1, r_f=1}^2 N(S_{fi, j_1} S_{fi, j_2}^*)_{4 \times 4}$, where S_{fi, j_1} and S_{fi, j_2} represent the scattering matrix elements with the emitted photon pair at helicity eigenstates j_1 and j_2 , and $j_1, j_2 = 1, 2, 3, 4$ correspond to the helicity eigenstates

$|++\rangle, |+-\rangle, |-+\rangle$, and $|--\rangle$, where \pm corresponds to the right/left-handed helicity [27]. N is chosen to keep $\text{Tr}[\rho_f] = 1$. r_i and r_f represent the spin of the electron at initial and final states, respectively, which have been traced out. The scattering matrix elements can be calculated for any choice of k_1, k_2 satisfying the constraint $(k_1 + k_2 - q_i - nk)^2 - m_*^2 = 0$.

In order to characterize the quantum entanglement of the emitted photon pair, we use the so-called concurrence as a measure of the entanglement [28]. The concurrence can be calculated from the density matrix as

$$\mathcal{C}(\rho_f) = \max(0, \sqrt{\zeta_1} - \sqrt{\zeta_2} - \sqrt{\zeta_3} - \sqrt{\zeta_4}), \quad (2)$$

where $\zeta_{1,2,3,4}$ are the 4 eigenvalues of the matrix $Q = \rho_f(\sigma^2 \otimes \sigma^2)\rho_f^*(\sigma^2 \otimes \sigma^2)$ in descending order, and σ^2 is one of the Pauli matrices. $\mathcal{C} \in [0, 1]$, with $\mathcal{C} = 0$ corresponding to a non-entangled state and $\mathcal{C} = 1$ corresponding to a fully entangled state. As the helicity of massless particles like photons are Lorentz invariant, the density matrix and the concurrence are also Lorentz invariant.

Microbunch enhancement

In the high-gain regime of FEL, a coherent enhancement due to the electron microbunching plays a vital role. For a sufficiently bright electron beam and a sufficiently long undulator, the combination of the undulator field and the radiation field will induce a ponderomotive potential modulating the energy of the electron beam [24]. This energy modulation eventually forces the electrons to form periodic microbunches along the undulator axis with a modulation wavelength $\lambda_1 = 2\pi/\omega_{fd}$ equal to the fundamental wavelength.

The conventional analysis of the coherence property due to the microbunching relies on paraxial wave equation [24], which cannot explain the quantum phenomenon of entangled photon pair emission. To overcome this problem, we develop a quantum collective double emission (QCDE) theory (see details in Section IV of SI). For simplicity, here we illustrate the physical picture of the coherent enhancement via an analogy with the quasi-phase-matching in nonlinear optics (see details in Section IV.D of SI).

In the electron frame, we can view the quasi-EM wave generated by the relativistic undulator as the pump and the emitted photon pair as signal and idler. The electron microbunches can be regarded as a nonlinear medium with periodic structure. Therefore, the phase difference between photons emitted by adjacent microbunches should be equal to $\Delta\phi = \Delta\mathbf{l} \cdot \Delta\mathbf{k}$, where $\Delta\mathbf{l} = |\Delta\mathbf{l}|\hat{\mathbf{e}}^3 = (\lambda_u/\gamma)(1 + K^2)/(2 + K^2)|\hat{\mathbf{e}}^3$ is the average relative displacement between adjacent microbunches, with $\hat{\mathbf{e}}^3$ being the unit vector along the undulator, and $\Delta\mathbf{k} = \mathbf{k}_1 + \mathbf{k}_2 - n\mathbf{k}$ is the momentum transfer between the pump photon and the emitted photon pair.

If the momenta of the signal and idler photons are both along the x^3 axis, the total momentum of the photon pair is $\mathbf{k}_1 + \mathbf{k}_2 = -n\mathbf{k}/(1 + K^2)$. Therefore the phase difference is exactly $\Delta\phi = 2\pi n$, resulting in a fully constructive interference between emissions from different electron microbunches and hence

an N_e^2 enhancement of the collective emission rate. In a practical FEL system, the situation deviates from the ideal one, and only adjacent microbunches within the coherence length contribute to the constructive interference, the number of which is estimated to be about $N_c = 22$ for the parameters shown in Table 1.

Meanwhile, if the directions of the emitted photon pair are away from the x^3 axis, the phase difference will deviate from $2\pi n$ with a nontrivial angular dependence

$$\Delta\phi(Z'_1, Z'_2, k_1^0) = 2\pi \left[(1 + K^2) \times \frac{1 + \cos(Z'_2) - (\cos(Z'_2) - \cos(Z'_1))k_1^0/k^0}{2 + K^2(1 + \cos(Z'_2))} \right] \quad (3)$$

(see details in Section IV of SI), where Z'_1, Z'_2 are the zenith angles of the two emitted photons relative to the x^3 axis in the electron frame. The enhancement parameter becomes $H(Z'_1, Z'_2, k_1^0) = \sum_{j=1}^{N_c} N_j e^{i[j\Delta\phi(Z'_1, Z'_2, k_1^0)]}$, where N_j is the number of electrons within the j^{th} electron microbunches. The collective emission rate is the multiplication of the emission rate from a single electron and the enhancement factor $|H(Z'_1, Z'_2, k_1^0)|^2$. Using the Lorentz transformation relationship $\gamma \tan(Z_l) = \sin(Z'_l)/(\beta + \cos(Z'_l))$, we can obtain the angles Z_1 and Z_2 in the lab frame for observation of the entangled photon pair emission.

Numerical results

We first calculate the total scattering rate \dot{W}_{fi} . We set practical ranges of photon energies and angular directions for both photon detectors, and focus on the case of $n = 1$. The relevant angles are illustrated in Fig. 2a. For the helical undulator, the dependence on the azimuthal angles A_1, A_2 of the emitted photon pair is simplified to $A_2 - A_1$. Thus, $d\dot{W}/dk_1^0 d\Omega_{k_1} d\Omega_{k_2}$ can be displayed in a three-dimensional space of the zenith angles Z_1, Z_2 and $A_2 - A_1$. Choosing $\omega_1 \simeq \omega_{\text{fd}}/3$ and $\omega_2 \simeq 2\omega_{\text{fd}}/3$ in the lab frame, the double angular distribution of the differential scattering rate $d\dot{W}/dk_1^0 d\Omega_{k_1} d\Omega_{k_2}$ is shown in Fig. 2b.

To demonstrate the quantum entanglement, we show the concurrence \mathcal{C} of the emitted photon pairs in Fig. 2c. Especially, \mathcal{C} can reach its upper limit of 1 for certain angles, meaning that fully-entangled two-photon states may be generated. Concurrence close to 1 can be approached at multiple angles. However, for most regions in the double-angular parameter space, the concurrence is relatively low. Thus, without selection or purification, the overall entanglement of the emitted photon pairs would vanish. In the next section, we will show how to improve the concurrence as an entangled photon pair source for experimental applications.

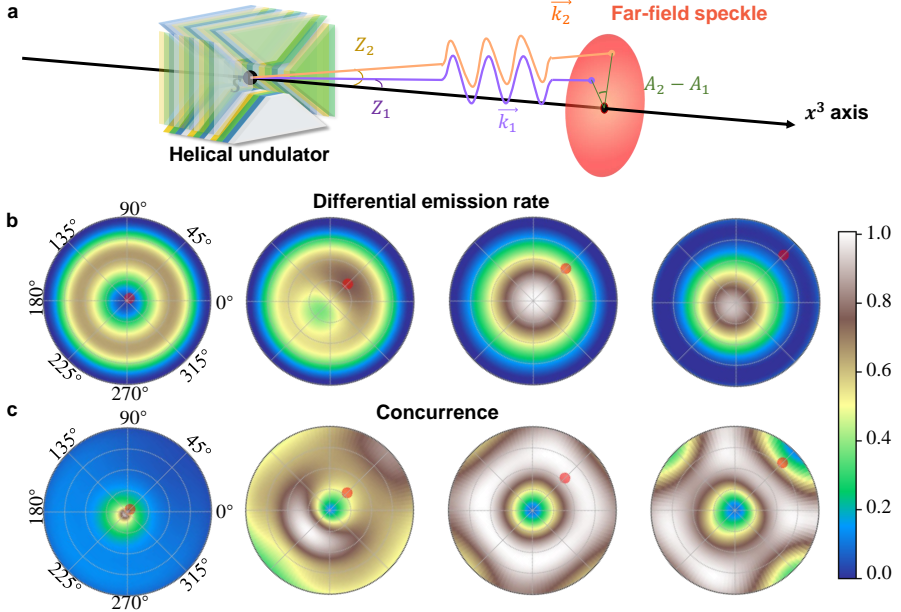


Fig. 2 Numerical simulation of entangled X-ray photon pair emission with microbunch enhancement. **a**, Illustration of the angles in **b** and **c**. $Z_{1,2}$ refer to the zenith angle between the three-momentum \vec{k}_1, \vec{k}_2 of the emitted photons and the x^3 axis. $A_2 - A_1$ is the difference between the azimuth angles of the emitted photons at the transverse far-field plane. Photons are treated as being emitted from the point S at the center of undulator for far-field measurement. **b**, Normalized double-angular distribution of the differential scattering rate $d\dot{W}/dk_1^0 d\Omega_{k_1} d\Omega_{k_2}$ in the lab frame. **c**, Double-angular distribution of the concurrence \mathcal{C} . In both **b** and **c**, the polar angles refers to $A_2 \in [0, 2\pi]$, and the radii refers to $\gamma \tan(Z_2) \in [0, 1]$ for photon 2. The red points represent the directions of photon 1. Here we choose $\omega_1 \simeq \omega_{fd}/3$.

Observation of entangled photon pairs

For potential applications in X-ray quantum optics, we aim to produce entangled photon pairs at certain 2-qubit states. In Fig. 3a, we show the proposed experimental scheme for the observation of the entangled photon pair emission. A variable line spacing (VLS) grating spectrometer used in the spectral analysis of the FEL [29, 30] can diffract the incident FEL beam to different orders (see Section X of SI for details). We can observe the 1st-order diffracted beams by placing two detectors with certain spectral response at certain positions along the focal plane.

For entanglement purification, we insert a circular aperture into the system as shown in Fig. 3a. The position of the circular hole is chosen to maximize the concurrence of the photon pairs that pass it, according to the numerical calculation for the angular distribution of concurrence shown in Fig. 2b. Specifically, concurrence close to 1 can be achieved at multiple angles such as

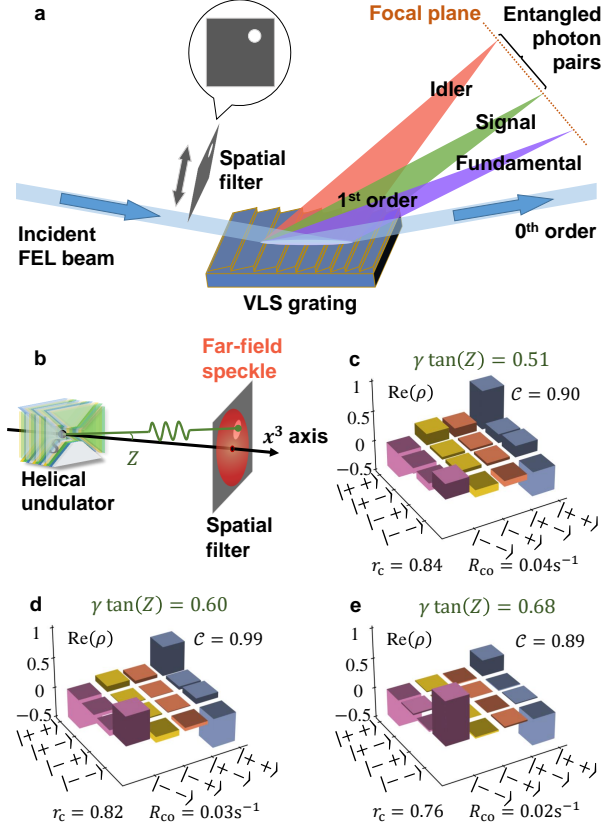


Fig. 3 Experimental scheme for the observation of entangled photon pairs. **a**, Experimental scheme based on variable line spacing (VLS) grating spectrometer in XFEL devices [29]. The signal and idler beams of the double-photon emission are separated and collected by two detectors at the focal plane. By inserting a circular aperture, the concurrence of the photon pair can be significantly increased. **b**, A detailed geometry of the aperture, where Z describes the angular position of the circular hole relative to the equivalent source point S . **c, d, e**, Real parts of the density matrices of the resulting entangled states for the aperture shown in **b** with sufficiently small hole and $\gamma \tan(Z) = 0.51, 0.60, 0.68$, which leads to $C = 0.90, 0.99, 0.89$, respectively. We also show the corresponding values of the effective coincidence ratio r_c and the coincidence count rate R_{co} for a 1 MHz electron source. The imaginary parts of the density matrices are zero due to the specific choice of the helicity basis and the identical emitting directions of the entangled photons (see Section VIII of SI for details).

$\gamma \tan(Z) = 0.51, 0.60, 0.68$ with sufficiently small aperture. A detailed geometry of the aperture and the resulting entangled states are displayed in Fig. 3b and Fig. 3c-e, respectively.

As the output photon pulse in our case has a time width of ~ 100 fs, which is much shorter than the temporal resolution of any current X-ray photon detector, we need to ensure the emission rate of entangled photon pairs in selected energy ranges to be less than 1 pair per electron pulse without the help

of the circular aperture, in order to make a time-coincidence detection of the entangled photon pairs. In addition, we need to depress the noise of accidental coincidence, which corresponds to two photons from different double emission processes being detected simultaneously or from single emission processes. To quantify the noise, we introduce an effective coincidence ratio r_c that represents the proportion of the entangled photon pairs to the total coincidence count rate R_{co} that refers to the photon pair detection rate of the two detectors, as shown in Fig. 3c-e (see Section V of SI for details).

Based on the experimental scheme above, an electron source with a repetition rate of 1 MHz as in the design of LCLS-II-HE or EuXFEL [31] can produce entangled photon pairs with a rate of $R_{co} \sim 10^{-2} \text{ s}^{-1}$ and an effective coincidence ratio $r_c \sim 0.8$, which can be used for X-ray quantum optical experiments.

Conclusion

In conclusion, we have theoretically demonstrated the entangled photon pair generation with FEL. In the electron frame, the double photon emission can be understood as the scattering between the electrons and the quasi-EM wave of the undulator field, which can be enhanced by the electron microbunching in FEL. We also propose an experimental scheme for the observation of the entangled photon pair emission. Our work shows that FEL can be utilized as an entangled photon pair source for X-ray quantum optics, which is impossible from a classical perspective.

Methods

We use the Floquet expansion of Volkov state in the the calculation of double emission scattering matrix S_{fi} . As the dependence of the Volkov wave function on the phase ϕ (thus four-position x) shows a periodicity of 2π , a Fourier expansion can be performed such that

$$\Psi_p^V(x) = \sum_{\vec{n}=-\infty}^{+\infty} F_{\vec{n}} e^{-i(q \cdot x + \vec{n} \cdot \vec{k} \cdot x)} u(p) . \quad (4)$$

Thus, the contributions to S_{fi} can be divided according to the number of Floquet photons absorbed, n . E.g., for the Feynman diagram shown in Fig. 1c,

$$\begin{aligned}
S_{\text{fi}} &= \int d^4x_1 \int d^4x_2 \bar{\Psi}_{\text{f}}^{\text{V}}(x_2) (-ie\mathcal{A}_2(x_2)) \\
&\quad \times (iG_{\text{V}}(x_2, x_1)) (-ie\mathcal{A}_1(x_1)) \Psi_{\text{i}}^{\text{V}}(x_1) \\
&\quad + \int d^4x_1 \int d^4x_2 \bar{\Psi}_{\text{f}}^{\text{V}}(x_2) (-ie\mathcal{A}_1(x_2)) \\
&\quad \times (iG_{\text{V}}(x_2, x_1)) (-ie\mathcal{A}_2(x_1)) \Psi_{\text{i}}^{\text{V}}(x_1) \\
&= -i \frac{e^2}{2V} \sqrt{\frac{1}{k_2^0 k_1^0}} \sum_{n=-\infty}^{+\infty} \left\{ \sum_{n_1=-\infty}^{+\infty} M_{\text{S}}(n, n_1) \right\} \Big|_{\text{MC}(n_1)} \\
&\quad \times (2\pi)^4 \delta^{(4)}(q_{\text{f}} + k_1 + k_2 - q_{\text{i}} - nk) \Big\} ,
\end{aligned} \tag{5}$$

where the helicity-relevant part $M_{\text{S}}(n, n_1)|_{\text{MC}(n_1)}$ is explained in Section II of SI, which only survives when momentum conservation is fulfilled at each vertex of the Feynman diagrams.

The differential scattering rate is then calculated by considering the total scattering probability \dot{W} of double emission that satisfies

$$\begin{aligned}
\dot{W} &= \int V \frac{d^3\mathbf{q}_{\text{f}}}{(2\pi)^3} V \frac{d^3\mathbf{k}_1}{(2\pi)^3} V \frac{d^3\mathbf{k}_2}{(2\pi)^3} \frac{|S_{\text{fi}}|^2}{VT} V \\
&= \int \frac{4V^4}{(2\pi)^9} d^3\mathbf{q}_{\text{f}} \int d\Omega_{k_1} \int d\Omega_{k_2} \int_0^{+\infty} dk_1^0 \int_0^{+\infty} dk_2^0 (k_1^0)^2 (k_2^0)^2 \frac{|S_{\text{fi}}|^2}{VT} ,
\end{aligned} \tag{6}$$

where VT is the space-time volume of the interaction zone. Combining Eq. 5 and Eq. 6, and completing the integral over variables except for k_1^0 , Ω_{k_1} and Ω_{k_2} , we obtain

$$\begin{aligned}
\frac{d\dot{W}}{dk_1^0 d\Omega_{k_1} d\Omega_{k_2}} &= \frac{e^4}{(2\pi)^5} \frac{m^2}{2q_{\text{i}}^0} \\
&\quad \times \sum_{n=1}^{+\infty} \frac{k_1^0 (k_2^0)^2 \Theta(q_{\text{i}}^0 + nk^0 - k_1^0 - k_2^0) M}{2|(q_{\text{i}} + nk - k_1) \cdot k_2|} \Big|_{\text{DE}(n)} ,
\end{aligned} \tag{7}$$

where $|_{\text{DE}(n)}$ means the constraint of $(q_{\text{i}} + nk - k_1) \cdot k_2 = q_{\text{i}} \cdot nk - q_{\text{i}} \cdot k_1 - nk \cdot k_1$, and the helicity-relevant part M is explained in Section II of SI.

The helical undulator simplifies the dependence of the double-emission process on the emitting azimuth angles A_1, A_2 to $A_2 - A_1$ and reduces the parameter space, making it more convenient to optimize the detection scheme for the entangled photon pairs in experiment. A detailed calculation for the case of linearly polarized undulator is given in Section VI in SI.

We represent the density matrix and the concurrence of the 2-qubit states of the emitted photon pairs with the basis of the helicity eigenstates

$|++\rangle, |+-\rangle, |-+\rangle, |--\rangle$. Alternatively, we can choose other basis states, such as linear polarization eigenstates [27], which result in a unitary transformation of the density matrix, and the concurrence remains invariant (see Section VII of SI for details). In addition, we can choose other entanglement monotones instead of the concurrence to quantify the entanglement degree, such as entanglement of formation and negativity. A comparison showing qualitative agreement between these entanglement measures and the concurrence is given in Section IX of SI.

Data availability

The data that support the findings of this study are available from the corresponding authors upon reasonable request.

Code availability

The code for the simulation is available from the corresponding authors upon reasonable request.

Acknowledgement

The authors are thankful to Zhirong Huang and Zhaoheng Guo for helpful discussions. This work was supported by the National Natural Science Foundation of China (No. 12174009, 11974031, 12174011).

References

- [1] Einstein, A., Podolsky, B., Rosen, N.: Can quantum-mechanical description of physical reality be considered complete? *Phys. Rev.* **47**(10), 777 (1935)
- [2] Bell, J.S.: On the problem of hidden variables in quantum mechanics. *Rev. Mod. Phys.* **38**(3), 447 (1966)
- [3] Shwartz, S., Coffee, R.N., Feldkamp, J.M., Feng, Y., Hastings, J.B., Yin, G.Y., Harris, S.E.: X-ray parametric down-conversion in the Langevin regime. *Phys. Rev. Lett.* **109**(1), 013602 (2012)
- [4] Emma, P., Akre, R., Arthur, J., Bionta, R., Bostedt, C., Bozek, J., Brachmann, A., Bucksbaum, P., Coffee, R., Decker, F.J., *et al.*: First lasing and operation of an ångstrom-wavelength free-electron laser. *Nature Photon.* **4**(9), 641–647 (2010)

- [5] Ishikawa, T., Aoyagi, H., Asaka, T., Asano, Y., Azumi, N., Bizen, T., Ego, H., Fukami, K., Fukui, T., Furukawa, Y., *et al.*: A compact X-ray free-electron laser emitting in the sub-ångström region. *Nature Photon.* **6**(8), 540–544 (2012)
- [6] Allaria, E., Castronovo, D., Cinquegrana, P., Craievich, P., Dal Forno, M., Danailov, M.B., D’Auria, G., Demidovich, A., De Ninno, G., Di Mitri, S., *et al.*: Two-stage seeded soft-X-ray free-electron laser. *Nature Photon.* **7**(11), 913–918 (2013)
- [7] Wang, W., Feng, K., Ke, L., Yu, C., Xu, Y., Qi, R., Chen, Y., Qin, Z., Zhang, Z., Fang, M., *et al.*: Free-electron lasing at 27 nanometres based on a laser wakefield accelerator. *Nature* **595**(7868), 516–520 (2021)
- [8] Pompili, R., Alesini, D., Anania, M.P., Arjmand, S., Behtouei, M., Bellaveglia, M., Biagioni, A., Buonomo, B., Cardelli, F., Carpanese, M., *et al.*: Free-electron lasing with compact beam-driven plasma wakefield accelerator. *Nature* **605**(7911), 659–662 (2022)
- [9] Duris, J., Li, S., Driver, T., Champenois, E.G., MacArthur, J.P., Lutman, A.A., Zhang, Z., Rosenberger, P., Aldrich, J.W., Coffee, R., *et al.*: Tunable isolated attosecond X-ray pulses with gigawatt peak power from a free-electron laser. *Nature Photon.* **14**(1), 30–36 (2020)
- [10] Duris, J.P., MacArthur, J.P., Glowina, J.M., Li, S., Vetter, S., Miahnahri, A., Coffee, R., Hering, P., Fry, A., Welch, M.E., *et al.*: Controllable x-ray pulse trains from enhanced self-amplified spontaneous emission. *Phys. Rev. Lett.* **126**(10), 104802 (2021)
- [11] Seibert, M.M., Ekeberg, T., Maia, F.R.N.C., Svenda, M., Andreasson, J., Jönsson, O., Odić, D., Iwan, B., Rocker, A., Westphal, D., *et al.*: Single mimivirus particles intercepted and imaged with an X-ray laser. *Nature* **470**(7332), 78–81 (2011)
- [12] Loh, N.D., Hampton, C.Y., Martin, A.V., Starodub, D., Sierra, R.G., Barty, A., Aquila, A., Schulz, J., Lomb, L., Steinbrener, J., *et al.*: Fractal morphology, imaging and mass spectrometry of single aerosol particles in flight. *Nature* **486**(7404), 513–517 (2012)
- [13] Gomez, L.F., Ferguson, K.R., Cryan, J.P., Bacellar, C., Tanyag, R.M.P., Jones, C., Schorb, S., Anielski, D., Belkacem, A., Bernando, C., *et al.*: Shapes and vorticities of superfluid helium nanodroplets. *Science* **345**(6199), 906–909 (2014)
- [14] Kern, J., Alonso-Mori, R., Tran, R., Hattne, J., Gildea, R.J., Echols, N., Glöckner, C., Hellmich, J., Laksmo, H., Sierra, R.G., *et al.*: Simultaneous femtosecond X-ray spectroscopy and diffraction of photosystem II at

- room temperature. *Science* **340**(6131), 491–495 (2013)
- [15] Erk, B., Boll, R., Trippel, S., Anielski, D., Foucar, L., Rudek, B., Epp, S.W., Coffee, R., Carron, S., Schorb, S., *et al.*: Imaging charge transfer in iodomethane upon x-ray photoabsorption. *Science* **345**(6194), 288–291 (2014)
 - [16] Rudek, B., Son, S., Foucar, L., Epp, S.W., Erk, B., Hartmann, R., Adolph, M., Andritschke, R., Aquila, A., Berrah, N., *et al.*: Ultra-efficient ionization of heavy atoms by intense X-ray free-electron laser pulses. *Nature Photon.* **6**(12), 858–865 (2012)
 - [17] Vinko, S.M., Ciricosta, O., Cho, B.I., Engelhorn, K., Chung, H.-K., Brown, C.R.D., Burian, T., Chalupský, J., Falcone, R.W., Graves, C., *et al.*: Creation and diagnosis of a solid-density plasma with an X-ray free-electron laser. *Nature* **482**(7383), 59–62 (2012)
 - [18] Fletcher, L.B., Lee, H.J., Döppner, T., Galtier, E., Nagler, B., Heimann, P., Fortmann, C., LePape, S., Ma, T., Millot, M., *et al.*: Ultrabright X-ray laser scattering for dynamic warm dense matter physics. *Nature Photon.* **9**(4), 274–279 (2015)
 - [19] Ciricosta, O., Vinko, S.M., Barbrel, B., Rackstraw, D.S., Preston, T.R., Burian, T., Chalupský, J., Cho, B.I., Chung, H.-K., Dakovski, G.L., *et al.*: Measurements of continuum lowering in solid-density plasmas created from elements and compounds. *Nat. Commun.* **7**(1), 1–6 (2016)
 - [20] Pellegrini, C., Marinelli, A., Reiche, S.: The physics of x-ray free-electron lasers. *Rev. Mod. Phys.* **88**(1), 015006 (2016)
 - [21] Lutman, A.A., MacArthur, J.P., Ilchen, M., Lindahl, A.O., Buck, J., Coffee, R.N., Dakovski, G.L., Dammann, L., Ding, Y., Dürr, H.A., *et al.*: Polarization control in an X-ray free-electron laser. *Nature Photon.* **10**(7), 468–472 (2016)
 - [22] Madey, J.M.J.: Stimulated emission of bremsstrahlung in a periodic magnetic field. *J. Appl. Phys.* **42**(5), 1906–1913 (1971)
 - [23] Temnykh, A.B.: Delta undulator for Cornell energy recovery linac. *Phys. Rev. ST Accel. Beams* **11**(12), 120702 (2008)
 - [24] Huang, Z., Kim, K.: Review of x-ray free-electron laser theory. *Phys. Rev. ST Accel. Beams* **10**(3), 034801 (2007)
 - [25] Ritus, V.I.: Quantum effects of the interaction of elementary particles with an intense electromagnetic field. *J. Sov. Laser Res.* **6**, 497–617 (1985)

- [26] Lötstedt, E., Jentschura, U.D.: Nonperturbative treatment of double Compton backscattering in intense laser fields. *Phys. Rev. Lett.* **103**(11), 110404 (2009)
- [27] Lötstedt, E., Jentschura, U.D.: Correlated two-photon emission by transitions of Dirac-Volkov states in intense laser fields: QED predictions. *Phys. Rev. A* **80**(5), 053419 (2009)
- [28] Wootters, W.K.: Entanglement of formation of an arbitrary state of two qubits. *Phys. Rev. Lett.* **80**(10), 2245 (1998)
- [29] Brenner, G., Kapitzki, S., Kuhlmann, M., Ploenjes, E., Noll, T., Siewert, F., Treusch, R., Tiedtke, K., Reininger, R., Roper, M.D., *et al.*: First results from the online variable line spacing grating spectrometer at FLASH. *Nucl. Instrum. Meth. A* **635**(1), 99–103 (2011)
- [30] Serkez, S., Krzywinski, J., Ding, Y., Huang, Z.: Soft x-ray self-seeding simulation methods and their application for the Linac Coherent Light Source. *Phys. Rev. ST Accel. Beams* **18**(3), 030708 (2015)
- [31] Decking, W., Abeghyan, S., Abramian, P., Abramsky, A., Aguirre, A., Albrecht, C., Alou, P., Altarelli, M., Altmann, P., Amyan, K., *et al.*: A MHz-repetition-rate hard X-ray free-electron laser driven by a superconducting linear accelerator. *Nature Photon.* **14**(6), 391–397 (2020)